Published in final edited form as:

Nat Cell Biol. 2011 April ; 13(4): 351–360. doi:10.1038/ncb2183.

Nde1-mediated inhibition of ciliogenesis affects cell cycle re-entry

Sehyun Kim[1], **Norann A. Zaghloul**[2,4], **Ekaterina Bubenshchikova**[1], **Edwin C. Oh**[2,4], **Susannah Rankin**[1,3], **Nicholas Katsanis**[2,4], **Tomoko Obara**[1], and **Leonidas Tsiokas**[1]

[1] Department of Cell Biology, University of Oklahoma Health Sciences Center, 975 NE 10th Street, Oklahoma City, Oklahoma 73104, USA

[2] McKusick-Nathans Institute of Genetic Medicine, Departments of Ophthalmology, Molecular Biology and Genetics, Johns Hopkins University School of Medicine, 733 North Broadway, Baltimore, Maryland 21205, USA

[3] Department of Cell Cycle and Cancer Biology, Oklahoma Medical Research Foundation, Oklahoma city, Oklahoma 73114, USA

Abstract

The primary cilium is an antenna-like organelle that is dynamically regulated during the cell cycle. Ciliogenesis is initiated as cells enter quiescence, while cilium resorption precedes mitosis. The mechanisms coordinating ciliogenesis with the cell cycle are unknown. Here we identify the centrosomal protein, Nde1, as a negative regulator of ciliary length. Nde1 is expressed at high levels in mitosis, low levels in quiescence and localizes at the mother centriole, which nucleates the primary cilium. Cells depleted of Nde1 show longer cilia and a delay in cell cycle re-entry that correlates with ciliary length. Knockdown of Nde1 in zebrafish embryos results in increased ciliary length, suppression of cell division, reduction of the number of cells forming the Kupffer's vesicle, and left-right patterning defects. These data suggest that Nde1 is an integral component of a network coordinating ciliary length with cell cycle progression and have implications in the transition from quiescence to a proliferative state.

More than thirty years ago, Tucker, Jensen, Biesele and colleagues made the seminal observations that "centriole ciliation" is associated with quiescence [1], [2], while deciliation is associated with entry into the cell cycle [3], [4]. It is now recognized that almost all ciliated cells follow this paradigm with ciliogenesis and cell cycle progression being mutually exclusive

Correspondence should be addressed to L.T. (leonidas-tsiokas@ouhsc.edu).

[4]Present address: University of Maryland School of Medicine, Department of Medicine, Division of Endocrinology, Diabetes and Nutrition, 660 W. Redwood Street, Baltimore, Maryland 21201 (NAZ); Department of Cell Biology and Center for Human Disease Modeling, Duke University Medical Center, Durham, North Carolina 27710 (ECO and NK).

Author Contributions

SK, NAZ, EB, EO, SR performed experiments. SK, NAZ, EB, SR, NK, TO, LT analyzed data. SK and LT planed the project. SK and LT wrote the manuscript.

Competing Financial Interest statement

None

processes [5], [6]. However, the molecular mechanisms coordinating these two processes are only recently starting to emerge. Much of the evidence connecting the two processes comes from observations that ciliary and centrosomal proteins can affect both the cilia and the cell cycle. Specifically, IFT88/polaris and IFT27 [7], [8], which are components of the intraflagellar transport machinery required for assembly of cilium/flagellum [9], have also effects on the cell cycle. Mutations in the ciliary phosphatase Inpp5E result in cilium destabilization and faster cell cycle re-entry in response to growth factor stimulation [10], [11]. Ciliary resorption mediated through a HEF1-Aurora A-HDAC6-dependent mechanism precedes cell cycle re-entry [12]. Centrosomal protein CP110 suppresses ciliogenesis through interactions with Cep97, CEP290, and Rab8a [13], [14] or centriolar length through interactions with CPAP [15–17]. The expression of both CP110 and CPAP is cell cycle-dependent [16], [18]. The cell cycle-regulated protein, Missing-in-Metastasis (MIM), functions antagonistically to the actin regulator cortactin to maintain a normal level of ciliogenesis [19]. Finally, a subset of centrosomal proteins have been shown to be required for both cell cycle progression and ciliogenesis [20].

Nuclear distribution gene E (NudE) was first identified in the filamentous fungus, *Aspergillus nidulans*, as an essential component in nuclear migration via a genetic interaction with the dynein holocomplex [21]. The mammalian ortholog of NudE, Nde1, is a centrosomal phosphoprotein with reported roles in mitosis [22–25] and interphase [26], [27]. Homozygous deletion of *Nde1* in mice causes microcephaly due to impaired cortical neurogenesis [23].

Results

Nde1 negatively regulates ciliary length

Immunofluorescence staining of Nde1 in NIH-3T3 cells revealed expression at one of the two centrioles (Fig. 1a). To test for a possible role of Nde1 in ciliogenesis, Nde1 was knocked down in NIH-3T3 cells by stable integration of a shRNA construct. Two cell lines, NIH-3T3$^{Nde1\text{-}KD1}$ and NIH-3T3$^{Nde1\text{-}KD2}$, were generated with different levels of Nde1 knockdown (Fig. 1b). Cilium formation in NIH-3T3^{WT} and NIH-3T3$^{Nde1\text{-}KD2}$ cells was induced by serum starvation. At all time points following serum starvation, NIH-3T3$^{Nde1\text{-}KD2}$ cells had longer cilia compared to NIH-3T3^{WT} cells (Fig. 1c; Supplementary information, Fig. S1a-d). Partial depletion of Nde1 in NIH-3T3$^{Nde1\text{-}KD1}$ cells had an intermediate effect on cilium length, between that observed in NIH-3T3^{WT} and NIH-3T3$^{Nde1\text{-}KD2}$ cells (Supplementary Information, Fig. S1a-d). Transient knockdown of mouse Nde1 in freshly isolated primary embryonic cortical neurons or human Nde1 (hNde1^{KD}) in retinal pigment epithelial cells (RPE1-hTERT) resulted in similar results as in NIH-3T3$^{Nde1\text{-}KD2}$ cells (Fig. 1e-i). To test whether depletion of Nde1 might have affected exit from the cell cycle that could account for the enhanced ciliogenesis, control or Nde1-depleted RPE1-hTERT cells were arrested in mitosis (M) and allowed to progress to G0. Ki-67 labeling, which marks cells in all phases of the cell cycle except G0, showed no difference in the percentage of cells exiting the cell cycle or entering G0 between control and Nde1-depleted RPE1-hTERT cells (Fig. 1j), suggesting that faster entry into G0 could not account for the formation of longer cilia induced by the depletion of Nde1.

To confirm the specificity of Nde1 knockdown on cilium formation, we expressed flag-tagged human Nde1 (f-hNde1) in NIH-3T3$^{Nde1\text{-}KD2}$ cells (Fig. 2a). Re-expression of Nde1 rescued ciliary length (Fig. 2b). Moreover, we observed that f-hNde1 had a dosage-dependent effect on ciliary length. Cells expressing the highest amount of f-hNde1 had stumpy cilia (Fig. 2c, panels *g*, *l*), while cells expressing the lowest levels of f-hNde1 had cilia of a size similar to NIH-3T3^{WT} cells (Fig. 2c, panels *c-d, h-i*). Intermediate levels of f-hNde1 expression showed bulged and stumpy cilia (Fig. 2c, panels *e-f, j-k*). As bulged cilia are also formed by loss-of-function mutations in subunits of dynein mediating intraflagellar transport (IFT) [28–30], we hypothesized that Nde1 may function antagonistically to the dynein complex in suppressing cilium length.

DYNLL1/LC8 as an effector of Nde1

The dynein light chain, DYNLL1/LC8 (LC8), has been shown to interact with Nde1 [22, 24]. LC8 also associates with retrograde IFT components [31] and is required for formation of flagella in *Chlamydomonas reinhardtii* [29]. In this organism, loss of LC8 leads to short or stumpy flagella [29], reminiscent of the short cilia we have seen upon Nde1 overexpression (Fig. 2c-d). To determine whether Nde1 exerts its ciliary effect through interaction with LC8, we engineered mutants of Nde1 that disrupt association with LC8. Nde1 contains two coiled-coil domains at its N-terminus that mediate homodimerization and interaction with Lis1 (Fig. 2e), the protein product of the gene mutated in type 1 lissencephaly, and a component of cytoplasmic dynein [32]. The centrosomal localization sequence and the LC8 binding domain in Nde1 have been loosely mapped at its C-terminus [24]. The N-terminal fragment of Nde1, Nde1$^{(1–180)}$, fails to localize at the centrosome, binds full-length Nde1, and functions as a dominant negative allele by sequestering endogenous Nde1 away from the centrosome [23]. It also fails to interact with LC8 (Supplementary information, Fig. S2b and 3). In a separate construct, we engineered two point mutations in the coiled-coil domains of Nde1, Nde1$^{(L135P/F138P)}$, that rendered Nde1 unable to homodimerize or interact with Lis1, but maintained interaction with LC8 (Supplementary information, Fig. S2c).

Cells transfected with Nde1$^{(1–180)}$ had abnormally long cilia, mimicking the ciliary phenotype of NIH-3T3$^{Nde1\text{-}KD2}$ cells (Fig. 2d; Supplementary information, Fig. S3a-b), while cells transfected with Nde1$^{(L135P,\ F138P)}$-myc showed stumpy cilia (Fig. 2f) similar to cells transfected with wild type Nde1 (Fig. 2d). These data suggest that the localization of Nde1 at the centrosome (basal body) and the C-terminus are essential for the suppression of cilium formation by Nde1 (Fig. 2g).

Because of the previously reported role of LC8 in flagella formation [29] and its ability to bind to the C-terminus of Nde1 (Supplementary information, Fig. S2), we first tested whether LC8 could modulate the ciliary phenotype induced by Nde1 overexpression. Transiently expressed f-LC8 accumulated at the base of the cilium and suppressed the effect of Nde1 on ciliary length (Fig. 3a). Consistently, overexpression or knockdown of LC8 resulted in longer or stumpy (or in some cells, loss of) cilia, respectively, in both NIH-3T3^{WT} and NIH-3T3$^{Nde1\text{-}KD2}$ cells (Fig. 3b-f), suggesting that LC8 might function downstream of Nde1 in regulating ciliary length. However, because LC8 overexpression did not quantitatively phenocopy the effect of Nde1 depletion on cilia (Figs. 1d and 3e), it is possible that Nde1

may regulate the activity of other proteins, in addition to LC8, to suppress ciliary length. In the case of LC8 though, one possibility would be that Nde1 regulates the amount of free LC8 through a physical interaction at the basal body. Thus, tethering LC8 at the basal body should result in short or no cilia.

To artificially tether LC8 at the basal body, we generated a chimeric construct in which the conserved LC8 binding motif, KSTQTQD [33] was fused to the centrosomal localization sequence of AKAP450 (PACT domain) [34] in a GFP expressing vector (GFP-PACT-LC8/BS). As control, we replaced the LC8 binding site from GFP-PACT-LC8/BS with an irrelevant sequence (GFP-PACT) and confirmed loss of LC8 binding activity (Supplementary information, Fig. S4a). Both GFP-PACT-LC8/BS and GFP-PACT in NIH-3T3^{WT} cells showed specific localization at the centrosome (Fig. 3g and h; Supplementary information, Fig. S4b). While overexpression of GFP-PACT in NIH-3T3^{WT} or NIH-3T3$^{Nde1\text{-}KD2}$ cells did not affect ciliary morphology (Fig. 3g; Supplementary information, Fig. S4b), overexpression of GFP-PACT-LC8/BS resulted in bulged or stumpy cilia (Fig. 3h; Supplementary information, Fig. S4b). Interestingly, overexpression of Nde1 or GFP-PACT-LC8/BS did not cause dispersion of the Golgi apparatus (Supplementary information, Fig. S5), as is caused by knockdown of LC8 [26], suggesting that the effects seen here are specific to the centrosomal/basal body pool of LC8. We conclude that Nde1 negatively regulates ciliary length by tethering endogenous LC8 at the basal body (Fig. 3i).

Cell cycle-dependent regulation of Nde1 levels

Because we have shown that Nde1 suppresses ciliary length, we examined its expression at the basal body during ciliation. In both NIH-3T3^{WT} and RPE1-hTERT cells, Nde1 expression gradually decreased over the course of serum starvation (Fig. 4a-e; Supplementary information, Fig. S6b). Conversely, serum re-stimulation resulted in the upregulation of Nde1, coinciding with the expression of G1/S markers (Fig. 4e; Supplementary information, Fig. S6d). To further test whether Nde1 levels were cell cycle-dependent, we used nocodazole to arrest cells in mitosis and then released them into the cell cycle in the presence of complete culture media. These experiments showed that Nde1 levels were increased in M and much reduced in G1 (Fig. 4f), consistent with a role as a suppressor of ciliogenesis.

Depletion of Nde1 causes a delay in cell cycle re-entry

Next, we examined the effect of Nde1 depletion on the cell cycle (Fig. 4g). Pulsed-labeling experiments using ethynyl-deoxyuridine (EdU) to identify DNA replicating cells, showed that knockdown of Nde1 resulted in a delay in EdU incorporation in NIH-3T3 or RPE1-hTERT cells (Fig. 5a, b, f, and g). Immunoblot analysis of cell cycle markers also showed a delay in G1/S transition of Nde1 depleted cells (Fig. 5h). Although ciliary resorption was evident in both NIH-3T3 and RPE1-hTERT EdU-positive cells (Fig. 5c, d, i, and j), it was not completed in NIH-3T3 cells, suggesting that initiation rather than complete ciliary resorption precedes DNA replication in NIH-3T3 and possibly, other mesenchymal cell types. Moreover, the fact that ciliary length was similar in EdU-positive wild type and NIH-3T3$^{Nde1\text{-}KD2}$ cells (Fig. 5e) implies that cilia of a certain, minimal length can be present during DNA replication in NIH-3T3 cells.

Cilia-mediated effect of Nde1 on cell cycle progression

To test whether the delayed entry to S in cells with reduced levels of Nde1 was mediated through the presence of long cilia *per se*, we determined whether this delay could be overcome in cells unable to form cilia by disrupting IFT. RNAi-mediated knockdown of IFT88/polaris or IFT20 in NIH-3T3 or RPE1-hTERT cells (Fig. 6a and b) suppressed cilia formation (Fig. 6c and d) and reversed the effect of Nde1 depletion on the rate of cell cycle re-entry (Fig. 6g and h), supporting the idea that Nde1 affected the rate of cell cycle re-entry through cilia.

It has been recently shown that an acute disruption of the actin cytoskeleton during serum starvation results in longer cilia [35]. We examined whether cytochalasin D (CD) treatment could induce a delay in G0/S progression that would be independent of Nde1 depletion. Fig. 6e and f show that simultaneous knockdown of Nde1 and disruption of actin cytoskeleton led to cilia longer than the cilia induced by the knockdown of Nde1 or disruption of actin cytoskeleton alone, indicating that Nde1 regulates ciliary length through a mechanism distinct from and synergistic with the mechanism induced by the disruption of the actin cytoskeleton. However, both modes of induction of longer cilia led to a delay in cell cycle re-entry (Fig. 6g).

Because disruption of the actin cytoskeleton by CD has been reported to arrest cells in G1/S transition [36], we tested whether acute CD treatment could delay the timing of cell cycle re-entry in cells depleted of IFT20. Treatment of $IFT20^{KD}$ RPE1-hTERT cells with CD did not have a significant effect on ciliation or the cell cycle profile during serum re-stimulation (Supplementary information, Fig. S7). These data suggest that the effect of a brief treatment of cells with CD on cell cycle re-entry is cilium-dependent in RPE1-hTERT cells.

Expression of a constitutively active form of the small GTPase Rab8a ($Rab8a^{Q67L}$) results in longer cilia [37]. However its effect on cell cycle re-entry is unknown. Consistent with our data that longer cilia delay cell cycle re-entry, $Rab8a^{Q67L}$ resulted in the formation of longer cilia (Fig. 6i) and a delayed entry into S (Fig. 6j). Altogether, these data showed that long cilia cause a delay in G0/S transition regardless of the means by which they were induced to form: depletion of Nde1, disruption of actin cytoskeleton, or stimulation of vesicle trafficking (Rab8a).

Nde1 controls ciliary length in zebrafish embryos

To test whether Nde1 has similar effects in the context of a living organism, we used zebrafish as a model system. The Kupffer's vesicle (KV) is a highly ciliated, transient organ that is essential for the initiation of left-right asymmetry in the zebrafish embryo [38]. It is formed by the initial migration of about two dozen dorsal forerunner cells at around somite stages (ss) 4–5 and persists until 14ss [38]. We tested whether knockdown of *nde1* could lead to longer cilia in cells forming the KV. We confirmed that *nde1* was expressed at the basal body in ciliated cells of the KV (data not shown). Fig. 7b and c show that depletion of zebrafish *nde1* resulted in longer cilia in both 6 and 10ss. These effects were specific to *nde1* depletion, as they were rescued by expression of the human *NDE1* mRNA (Fig. 7a). Moreover, we found that the size of the KV was smaller in the 10ss of *nde1* morphants

(*nde1* MO) (Fig. 7b and f). Staining for atypical Protein Kinase C (aPKC) which marks the surface of the cells forming the KV revealed that the KV in *nde1* MO consisted of a smaller number of cells compared to wild type vesicles, while the percentage of ciliated cells was similar (Fig. 7b-e). Since reduced number of cells in the KV can arise from defects in cell proliferation and/or increased cell death, we stained wild-type or *nde1* MO embryos with TUNEL or phosphorylated histone H3 (pH3), to identify apoptotic or mitotic cells, respectively. We did not see differences in TUNEL staining at the KV (Supplementary information, Fig. S8), but observed a reduction in the pH3-positive cells in *nde1* MO embryos at 10ss (Fig. 7f and g). These data led us to conclude that the KV consists of ~20 ciliated cells at early somitic stages and this cell population approximately doubles at later stages. Nde1 appears to be critical for the expansion of this cell population.

Ciliary defects induced by the depletion of Nde1 in zebrafish embryos

To determine whether depletion of Nde1 could result in left-right patterning defects, we examined the expression patterns of an early (*southpaw*) and late (*myl-7*) marker of left-right asymmetry in control and *nde1* MO. Fig. 7h shows that depletion of *nde1* resulted in the randomization of *southpaw* expression at the lateral plate mesoderm at 14 hours post-fertilization (hpf). Expression of *myl-7* at 48 hpf revealed a significant increase in the proportion of embryos showing leftward or no heart looping, both indicative of left-right patterning defects (Fig. 7i). Overall and in light of our cell culture data, we suggest that formation of longer cilia in *nde1* MO causes a delay in cell cycle progression, which in turn leads to a smaller KV due to a reduced number of cells forming the KV. This structural defect may account for the left-right patterning defects seen in *nde1* MO.

Discussion

In the present study, we provide evidence for a function of Nde1 in integrating ciliogenesis with the cell cycle. This conclusion is based on the following findings: First, Nde1 negatively regulates ciliary length through a mechanism involving LC8. Second, Nde1 localizes at the basal body/centriole during interphase and shows a cell cycle-dependent expression that inversely correlates with ciliogenesis. Third, depletion of Nde1 leads to a delay in G0/S transition that correlates to the length of the primary cilium. These data lead us to propose a model in which the cell cycle controls ciliogenesis through the regulation of Nde1 expression levels, while the primary cilium influences the timing of cell cycle re-entry through its physical length.

Nde1 can interact with several proteins. We present evidence for a functional role of the Nde1-LC8 interaction in ciliogenesis. LC8 is a component of the retrograde IFT in *Chlamydomonas reinhardtii* [22], [24], [29] where it is required for formation of flagella, and has been localized to the human ciliary axoneme [39]. Here we show that tethering LC8 at the basal body suppresses the effect of Nde1 depletion on cilia, and overexpression of LC8 suppresses the phenotype induced by Nde1 overexpression. These data lead us to conclude that LC8 is likely to be a proximal effecter of Nde1 in the regulation of ciliary length.

LC8 serves as a dimerization hub for proteins involved in several processes including organelle positioning [26]. We find that regulation of LC8 at the basal body by Nde1 serves a

specific role in the regulation of ciliary morphology. A loss-of-function mutation in the retrograde IFT component, dynein heavy chain 2 (*Dnchc2*) in mice results in stumpy cilia, which phenocopies Nde1 overexpression. Thus, we speculate that the Nde1-mediated sequestration of LC8 at the basal body may negatively regulate the ability of retrograde dynein to contribute to cilium formation.

The centrosome plays critical roles in both (de)ciliation and the cell cycle, specifically at the G1/S transition [20], [40]. It is possible that Nde1 independently affects both of these processes through its presence at the centrosome. Alternatively, Nde1 could affect cilia formation indirectly, through its effect on the cell cycle. Here we provide several lines of evidence suggesting that the role of Nde1 in cell cycle entry depends directly on ciliation. First, depletion of Nde1 did not affect mitotic exit and/or entry to G0 making it unlikely that depletion of Nde1 could have promoted ciliogenesis due to an indirect effect on the cell cycle. Second, 24h of serum starvation resulted in longer cilia in Nde1 depleted cells compared to wild-type, while the number of ciliated cells was identical. This suggests that increased ciliary length rather than percentage of ciliated cells would most likely account for the delay in cell cycle re-entry induced by the depletion of Nde1. Third, knockdown of IFT88/polaris or IFT20 not only led to loss of cilia in both wild type and Nde1 knockdown cells, but also rescued the delay in cell cycle reentry induced by the depletion of Nde1. While it could be argued that IFT88/polaris might have rescued the Nde1-induced delay in cell cycle progression through its previously reported extraciliary effects on G1 to S transition [8], this argument cannot be made for IFT20, which has a strictly IFT-specific function in cell culture [41], [42]. Finally, induction of longer cilia by the ectopic expression of the constitutively active variant of Rab8a (Rab8a^{Q67L}) or a brief disruption of the actin cytoskeleton, led to a delay in G1/S transition. Therefore, the Nde1-induced delay in cell cycle progression is most likely to be caused by the presence of abnormally long cilia.

The cellular consequences of abnormally long cilia have not previously been characterized. Here we show that they can influence the cell cycle by inducing a delay in G0/S transition. This observation has implications in the pathophysiology of microcephaly, a condition characterized by severe thinning of the later-formed superficial layers (II to IV) of the cerebral cortex. Deletion of *Nde1* in mice results in microcephaly [23]. This phenotype was originally explained by the mitotic defects caused by the loss of Nde1 leading to longer duration in neuronal progenitor cell division [23]. An alternative model suggested by our data predicts that an increase in ciliary length in *Nde1*$^{-/-}$ progenitor neurons may contribute to proliferative delays by prolonging exit from G1. This idea is supported by the formation of longer cilia in embryonic cortical neurons induced by the depletion of Nde1 and the formation of smaller heads in *nde1* MO (Supplementary information, Fig. S9). Moreover, hippocampal neurogenesis is profoundly increased in mice with a conditional knockout of *Stumpy* due to the loss of primary cilia in hippocampal precursors [43]. Furthermore, mice with the *Bbs1*$^{M390R/M390R}$ mutation knocked in, which represents the most common mutation in Bardet-Biedl syndrome patients, show thinning of the cerebral cortex resulting in microcephaly [44]. Strikingly, these mice have a mixed pool of abnormally long and short primary cilia in neuronal precursors suggesting that a subpopulation of neuronal cells,

perhaps the ones with longer primary cilia, may be responsible for the dysregulated neocortical development [44].

Methods

Cell culture

NIH-3T3, HEK293T and RPE1-hTERT cells were obtained from ATCC and maintained in Dulbecco's Modified Eagle's Medium (DMEM) plus 10% calf serum (NIH-3T3) or DMEM plus 10% fetal bovine serum (HEK293T and RPE1-hTERT). RPE1-hTERT cells with stable integration of a shRNA construct against IFT20 ($IFT20^{KD}$) were cultured in DMEM plus 10% fetal bovine serum (gift from Dr. Greg Pazour).

Primary embryonic neurons

E18.5 mouse embryonic brains were dissociated and prepared as described (Lonza); cortical neurons were resuspended in Neuron Nucleofector Solution and electroporated (Lonza) with GFP and an shRNA plasmid directed against mouse Nde1 and cultured in Neurobasal-A medium (Invitrogen) supplemented with GlutaMAX (Invitrogen) and B27 (Invitrogen). For immunofluorescence, cells were plated at a density of 100,000 cells per well in a 24 well plate containing poly-L-lysine-coated cover slips. Cultures were incubated in a humidified 37°C/5% CO2 incubator for 6 days before analysis. Transfected cortical neurons were identified by GFP- and doublecortin (DCX)- staining (goat α-DCX, Santa Cruz Biotechnology, 1:100) and primary cilia were visualized using a rabbit polyclonal antibody against adenylyl cyclase 3 (ACIII, Santa Cruz Biotechnology, 1:500).

Plasmids

Mouse and human Nde1 and human LC8 cDNA were obtained from Open Biosystems and was subcloned into a pFLAG-CMV-2 vector (Sigma). Mutant forms of Nde1 ($Nde1^{(1–180)}$ and $Nde1^{(L135P, F138P)}$) were generated using the QuikChange mutagenesis kit according to the manufacturer's instructions (Stratagene). $Rab8a^{Q67L}$-GFP was a gift from Dr. Johan Peränen. A construct containing the PACT domain was obtained from Dr. Sean Munro.

RNAi

A 64-mer mouse Nde1-specific oligomer (sense strand: 5′-GATCCCCGTTTGAGATGC AGCACTCATTCAAGAGATGAGTGCTGCATCTCAAACTTTTTGGAAA-3′) was used to generate a short hairpin Nde1 RNA construct. Mouse IFT88/polaris-specific siRNA (5′-CCAACGACCTGGAGATTAA-3′), mouse LC8-specific smart pool siRNA (5′-GGGAACACCUCGUUUGAAU-3′, 5′-UGUGUUGUGUACAGGGCUU-3′, 5′-GCACAUGAAACCAAACACU-3′, 5′-GUUCAAAUCUGGUUAAAAG-3′), human IFT88/polaris-specific smart pool siRNA (5′-AGUAAAGGUGAACGACUAA-3′, 5′-AGGAAGUGCUAGCGGUGAU-3′, 5′-AGGCAAAUGGAACGUGAAA-3′, 5′-GAGAAUUAUAUGAUGGUGA-3′), and human Nde1-specific smart pool siRNA (5′-GGACCCAGCUCAAGUUUAA-3′, 5′-GCGCAGACCAAAGCCAUUA-3′, 5′-GCUGAAGCCUGUUCUUGGU-3′, 5′-GCAGCACUCUGAAGGCUAC-3′) were obtained from Dharmacon (Thermo scientific).

Immunoblotting

NIH-3T3 and RPE1-hTERT cells were lysed in 1% Triton X-100, 150 mM NaCl, 10 mM Tris-HCl, pH 7.5, 1 mM EGTA, 1 mM EDTA, 10% sucrose, and protease inhibitor cocktail (Roche Applied Science) at 4 °C for 30 min. NE-PER nuclear and cytoplasmic extraction reagents (Thermo scientific) were used in both NIH-3T3 and RPE1-hTERT cells to obtain whole cell lysates, following manufacturer's instructions. Antibodies against Nde1 (Proteintech), IFT88/polaris (gift from Dr. Bradley Yoder), IFT20 (gift from Dr. Greg Pazour), $pRB^{S807/811}$ (Cell signaling technology), $pCdc2^{Y15}$ (Cell signaling technology), cyclin A (Abcam), cyclin E (Abcam), α-tubulin (Sigma-Aldrich) and β-actin (Sigma-Aldrich) were used at a 1:1000 dilution. LC8 (gift from Dr. Steven King or BD transduction laboratory) was used at 1:500. Densitometric quantification of autoradiograms was analyzed by Image J software.

Indirect immunofluorescence

Cells grown on glass coverslips were fixed in a 1:1 methanol/acetone, permeabilized in 0.2% Triton X-100 in phosphate buffered saline (PBS), blocked in 2% heat inactivated goat serum/0.2% Triton X-100 in PBS (blocking buffer), and incubated overnight with primary antibodies diluted in blocking buffer at 4 °C. Primary antibody against centrin2 was used at 1:500 (gift from Dr. Jeffrey Salisbury), acetylated α-tubulin at 1:1000 (Sigma-Aldrich), γ-tubulin at 1:1000 (Sigma-Aldrich), Nde1 at 1:250 (Proteintech), Flag at 1:1000 (Sigma-Aldrich), IFT88/Polaris at 1:500 (gift from Dr. Bradley Yoder), c-myc at 1:1000 (Santa Cruz biotechnology) and GM130 at 1:1000 (BD transduction laboratory). Cells were washed three times with PBS and incubated for 2h at 4 °C with appropriate combinations of fluorescence-labeled secondary antibodies at 1:2000 dilution. Secondary antibodies were donkey anti-rabbit Alexa 488, donkey anti-mouse Alexa 568, goat anti-mouse Alexa 488, goat anti-rabbit Alexa 568, donkey anti-mouse Alexa 568, or donkey anti-rabbit Alexa 647 (Molecular Probes Inc.). Excess of secondary antibodies was removed by four washes in PBS. DNA was stained with 5 μg/ml DAPI for 5 min. Coverslips were mounted with ProLong (Molecular Probes), images were acquired with a Leica SP2 MP confocal microscope, and processed with Leica confocal software (LCS Lite) and Adobe Photoshop 6.0.

Stable and transient transfections

NIH-3T3 cells were co-transfected with the mouse Nde1-specific or control shRNAi construct and pEYFP-C1 (BD Biosciences) using Lipofectamine PLUS (Invitrogen) in a 10:1 plasmid concentration ratio, respectively. Stable transfectants were selected in 500 μg/ml G418 and 10 μg/ml blasticidin for 3 weeks. Individual clones were isolated, expanded, and sorted for YFP positive cells using the Influx cell sorter (Cytopeia) to obtain pure populations of Nde1 shRNAi expressing cells. Individual clones were tested for Nde1 expression by immunoblotting and RT-PCR. Transient transfections in NIH-3T3 or RPE1-hTERT cells were done by Lipofectamine PLUS (Invitrogen) or DharmaFECT-Duo (Dharmacon-Thermo Fisher), whereas the calcium phosphate precipitation protocol was used in HEK293T cells.

Retroviral expression

Recombinant VSV-G pseudotyped retroviruses containing f-hNde1 or GFP were packaged in HEK393T cells by transient co-transfection of *gag-pol*, VSV-G, and pQCXIP (Clontech) containing f-hNde1 or pQCXIN (Clontech) containing GFP. Exponentially growing NIH-3T3^{WT} or NIH-3T3$^{Nde1\text{-}KD2}$ cells were infected with recombinant retroviruses for 8 h in the presence of 8 μg/ml polybrene. To ensure expression of f-hNde1 in all infected cells, the f-hNde1 cDNA was cloned in front of an internal ribosome entry site (IRES) followed by the puromycin resistance gene (pQCXIP vector) and infected cells were selected for 12 days in media containing puromycin (1 μg/ml). Pools of puromycin-resistant cells were expanded and expression of f-hNde1 was determined by α-flag or α-Nde1 by both Western blotting and indirect immunofluorescence. GFP positive cells were isolated by cell sorting (Influx cell sorter, Cytopeia). Ciliary length was determined by indirect immunofluorescence using 611B.

Cell cycle analysis

For analysis of cell DNA content, NIH-3T3 cells were fixed with 70% ethanol or 0.5% formaldehyde (Sigma-Aldrich) and stored in −20°C for no longer than 24h. After fixation, cells were stained with 20 μg/ml propidium iodide (Sigma-Aldrich) plus 200 μg/ml RNAase A (Sigma-Aldrich) in PBS and subjected to flow cytometry analysis. At least 10,000 cells were analyzed per sample using a FACS Calibur® cell cytometer. An alternative form of BrdU, EdU, was pulsed in serum starved or re-stimulated cells, 3 or 6h before fixation according to the manufacturer's instrucutions (Click-iT EdU assay kit, Invitrogen).

Inhibitors

For mitotic synchronization, NIH-3T3 or RPE1-hTERT cells were incubated for 12h in DMEM plus 10% calf serum (or fetal bovine serum) with 600 ng/ml nocodazole (Sigma) to arrest dividing cells in metaphase. Loosely attached, mitotic cells were shaken off the culture flask and collected. Next, the cells were washed with PBS to remove nocodazole and re-suspended in complete culture media (10% serum) for recovery. To acutely disrupt actin cytoskeleton, cytochalasin D (Sigma) or DMSO (Sigma) was used at 2.5 nM for 90 min during the 24h of serum starvation.

Zebrafish experiments

A translation blocking morpholino (MO) (5′-GGCTCTGGGTCA CTCATTGCTGTTC-3′) against endogenous zebrafish *nde1* (accession number: NM_001030203) was designed and obtained from Gene Tools LLC. A volume of 4.6 nl in a concentration of 1 ng/nl *nde1* morpholino was injected into one- to two-cell stage embryos using a nanoliter 2000 microinjector (World Precision Instrments). Full length human *NDE1* cDNA was cloned into pCS2+ for *in vitro* transcription using the SP6 mMessage mMachine Kit (Ambion). 50 pg of mRNA was injected either alone or with *nde1* MO. For immunofluorescence, the embryos were fixed with 4% formaldehyde in PBS at 4°C overnight and transferred to 100% MeOH for 2hrs at −20 °C followed by an overnight incubation at 4°C. After rehydrating the embryos, they were washed in PBS with 0.1% Tween-20 and blocked in PBS-DBT (1xPBS, 1% BSA, 1% DMSO, 10% normal goat serum and 0.1% Tween-20) at room temperature for

2 hours, followed by antibody staining with acetylated α-tubulin (1:1000, Sigma), phosphorylated histone H3 (1:750, Cell Signaling technology), atypical PKC (1:100, Santa Cruz biotechnology), or Nde1 (1:200, Proteintech) at 4 °C overnight. After 30 min, four washes in PBTw (1xPBS/0.1% Tween 20), the embryos were incubated with a goat anti-mouse Alexa Fluor 546 (1:1000, Molecular Probe) and goat anti-rabbit Alexa Fluor 488 (1:1000, Molecular Probes) for 2 hours at room temperature and washed in PBTw. Embryos were rinsed by 100% MeOH and cleared in a benzoyl-alchohol:benzoyl-benzoate (1:2) solution and viewed on a Leica SP2 MP confocal microscope and processed with Leica confocal software (LCS Lite). Ciliary length was measured using ImageJ software. Asymmetric gene expression was determined by whole-mount *in situ* hybridization using a *southpaw* or *myl-7* DIG-UTP at 14 or 48 hpf, respectively.

Statistics

Data are presented as mean ± SEM. Statistical difference between groups was determined by unpaired Student's *t* test. Two groups were considered different when *P* value was less than 0.05. *P* values less than 0.001 were indicated (Fig. 7).

Supplementary Material

Refer to Web version on PubMed Central for supplementary material.

Acknowledgments

We thank Drs. Joel Rosenbaum, Steve Doxsey, Chris Wood, Nedra Wilson, Dean Dawson, Scott Plafker, and Ralf Janknecht for comments on the manuscript, Sean Munro, Brad Yoder, Johan Peränen, Jeff Salisbury, Andrew S. McCallion, and Greg Pazour for reagents, and the Yost, Sive, Amack, and Zon labs for zebrafish immuno-staining protocols. This work was also supported by grants R01HD04260 from the National Institute of Child Health and Development (NK), R01DK072301, R01DK075972 (NK), R01DK078209 (TO) and R01DK59599 (LT) from the National Institute of Diabetes, Digestive and Kidney disorders, P20RR017703 from the National Center for Research Resources (LT), a Visual Neuroscience Training Program grant from the National Eye Institute (NAZ), HR06-175 (SR) and HR07-097 (LT) from the Oklahoma Center for the Advancement of Science and Technology, and the John S. Gammill Endowed Chair for PKD (LT). SR is a Pew Scholar in the Biomedical Sciences, supported by The Pew Charitable Trusts.

References

1. Rash JE, Shay JW, Biesele JJ. Cilia in cardiac differentiation. Journal of ultrastructure research. 1969; 29:470–484. [PubMed: 5365371]
2. Tucker RW, Pardee AB, Fujiwara K. Centriole ciliation is related to quiescence and DNA synthesis in 3T3 cells. Cell. 1979; 17:527–535. [PubMed: 476831]
3. Rieder CL, Jensen CG, Jensen LC. The resorption of primary cilia during mitosis in a vertebrate (PtK1) cell line. Journal of ultrastructure research. 1979; 68:173–185. [PubMed: 480410]
4. Tucker RW, Scher CD, Stiles CD. Centriole deciliation associated with the early response of 3T3 cells to growth factors but not to SV40. Cell. 1979; 18:1065–1072. [PubMed: 229969]
5. Pan J, Snell W. The primary cilium: keeper of the key to cell division. Cell. 2007; 129:1255–1257. [PubMed: 17604715]
6. Quarmby LM, Parker JD. Cilia and the cell cycle? J Cell Biol. 2005; 169:707–710. [PubMed: 15928206]
7. Qin H, Wang Z, Diener D, Rosenbaum J. Intraflagellar transport protein 27 is a small G protein involved in cell-cycle control. Curr Biol. 2007; 17:193–202. [PubMed: 17276912]

8. Robert A, et al. The intraflagellar transport component IFT88/polaris is a centrosomal protein regulating G1-S transition in non-ciliated cells. J Cell Sci. 2007; 120:628–637. [PubMed: 17264151]
9. Rosenbaum JL, Witman GB. Intraflagellar transport. Nat Rev Mol Cell Biol. 2002; 3:813–825. [PubMed: 12415299]
10. Bielas SL, et al. Mutations in INPP5E, encoding inositol polyphosphate-5-phosphatase E, link phosphatidyl inositol signaling to the ciliopathies. Nat Genet. 2009; 41:1032–1036. [PubMed: 19668216]
11. Jacoby M, et al. INPP5E mutations cause primary cilium signaling defects, ciliary instability and ciliopathies in human and mouse. Nat Genet. 2009; 41:1027–1031. [PubMed: 19668215]
12. Pugacheva EN, Jablonski SA, Hartman TR, Henske EP, Golemis EA. HEF1-dependent Aurora A activation induces disassembly of the primary cilium. Cell. 2007; 129:1351–1363. [PubMed: 17604723]
13. Spektor A, Tsang WY, Khoo D, Dynlacht BD. Cep97 and CP110 suppress a cilia assembly program. Cell. 2007; 130:678–690. [PubMed: 17719545]
14. Tsang WY, et al. CP110 suppresses primary cilia formation through its interaction with CEP290, a protein deficient in human ciliary disease. Dev Cell. 2008; 15:187–197. [PubMed: 18694559]
15. Schmidt TI, et al. Control of centriole length by CPAP and CP110. Curr Biol. 2009; 19:1005–1011. [PubMed: 19481458]
16. Tang CJ, Fu RH, Wu KS, Hsu WB, Tang TK. CPAP is a cell-cycle regulated protein that controls centriole length. Nat Cell Biol. 2009; 11:825–831. [PubMed: 19503075]
17. Kohlmaier G, et al. Overly long centrioles and defective cell division upon excess of the SAS-4-related protein CPAP. Curr Biol. 2009; 19:1012–1018. [PubMed: 19481460]
18. Chen Z, Indjeian VB, McManus M, Wang L, Dynlacht BD. CP110, a cell cycle-dependent CDK substrate, regulates centrosome duplication in human cells. Dev Cell. 2002; 3:339–350. [PubMed: 12361598]
19. Bershteyn M, Atwood SX, Woo WM, Li M, Oro AE. MIM and cortactin antagonism regulates ciliogenesis and hedgehog signaling. Dev Cell. 2010; 19:270–283. [PubMed: 20708589]
20. Mikule K, et al. Loss of centrosome integrity induces p38-p53-p21-dependent G1-S arrest. Nat Cell Biol. 2007; 9:160–170. [PubMed: 17330329]
21. Efimov VP, Morris NR. The LIS1-related NUDF protein of Aspergillus nidulans interacts with the coiled-coil domain of the NUDE/RO11 protein. J Cell Biol. 2000; 150:681–688. [PubMed: 10931877]
22. Feng Y, et al. LIS1 regulates CNS lamination by interacting with mNudE, a central component of the centrosome. Neuron. 2000; 28:665–679. [PubMed: 11163258]
23. Feng Y, Walsh CA. Mitotic spindle regulation by Nde1 controls cerebral cortical size. Neuron. 2004; 44:279–293. [PubMed: 15473967]
24. Stehman SA, Chen Y, McKenney RJ, Vallee RB. NudE and NudEL are required for mitotic progression and are involved in dynein recruitment to kinetochores. J Cell Biol. 2007; 178:583–594. [PubMed: 17682047]
25. Vergnolle MA, Taylor SS. Cenp-F links kinetochores to Ndel1/Nde1/Lis1/dynein microtubule motor complexes. Curr Biol. 2007; 17:1173–1179. [PubMed: 17600710]
26. Lam C, Vergnolle MA, Thorpe L, Woodman PG, Allan VJ. Functional interplay between LIS1, NDE1 and NDEL1 in dynein-dependent organelle positioning. J Cell Sci. 2010; 123:202–212. [PubMed: 20048338]
27. Shmueli A, et al. Ndel1 palmitoylation: a new mean to regulate cytoplasmic dynein activity. EMBO J. 29:107–119. [PubMed: 19927128]
28. May SR, et al. Loss of the retrograde motor for IFT disrupts localization of Smo to cilia and prevents the expression of both activator and repressor functions of Gli. Dev Biol. 2005; 287:378–389. [PubMed: 16229832]
29. Pazour GJ, Wilkerson CG, Witman GB. A dynein light chain is essential for the retrograde particle movement of intraflagellar transport (IFT). J Cell Biol. 1998; 141:979–992. [PubMed: 9585416]

30. Pazour GJ, Dickert BL, Witman GB. The DHC1b (DHC2) isoform of cytoplasmic dynein is required for flagellar assembly. J Cell Biol. 1999; 144:473–481. [PubMed: 9971742]
31. Rompolas P, Pedersen LB, Patel-King RS, King SM. Chlamydomonas FAP133 is a dynein intermediate chain associated with the retrograde intraflagellar transport motor. J Cell Sci. 2007; 120:3653–3665. [PubMed: 17895364]
32. McKenney RJ, Vershinin M, Kunwar A, Vallee RB, Gross SP. LIS1 and NudE induce a persistent dynein force-producing state. Cell. 2010; 141:304–314. [PubMed: 20403325]
33. Martinez-Moreno M, et al. Recognition of novel viral sequences that associate with the dynein light chain LC8 identified through a pepscan technique. FEBS Lett. 2003; 544:262–267. [PubMed: 12782328]
34. Gillingham AK, Munro S. The PACT domain, a conserved centrosomal targeting motif in the coiled-coil proteins AKAP450 and pericentrin. EMBO reports. 2000; 1:524–529. [PubMed: 11263498]
35. Kim J, et al. Functional genomic screen for modulators of ciliogenesis and cilium length. Nature. 464:1048–1051. [PubMed: 20393563]
36. Rubtsova SN, et al. Disruption of actin microfilaments by cytochalasin D leads to activation of p53. FEBS Lett. 1998; 430:353–357. [PubMed: 9688570]
37. Nachury MV, et al. A core complex of BBS proteins cooperates with the GTPase Rab8 to promote ciliary membrane biogenesis. Cell. 2007; 129:1201–1213. [PubMed: 17574030]
38. Essner JJ, Amack JD, Nyholm MK, Harris EB, Yost HJ. Kupffer's vesicle is a ciliated organ of asymmetry in the zebrafish embryo that initiates left-right development of the brain, heart and gut. Development. 2005; 132:1247–1260. [PubMed: 15716348]
39. Ostrowski LE, et al. A proteomic analysis of human cilia: identification of novel components. Mol Cell Proteomics. 2002; 1:451–465. [PubMed: 12169685]
40. Matsumoto Y, Maller JL. A centrosomal localization signal in cyclin E required for Cdk2-independent S phase entry. Science. 2004; 306:885–888. [PubMed: 15514162]
41. Baker SA, Freeman K, Luby-Phelps K, Pazour GJ, Besharse JC. IFT20 links kinesin II with a mammalian intraflagellar transport complex that is conserved in motile flagella and sensory cilia. J Biol Chem. 2003; 278:34211–34218. [PubMed: 12821668]
42. Follit JA, Tuft RA, Fogarty KE, Pazour GJ. The intraflagellar transport protein IFT20 is associated with the Golgi complex and is required for cilia assembly. Mol Biol Cell. 2006; 17:3781–3792. [PubMed: 16775004]
43. Breunig JJ, et al. Primary cilia regulate hippocampal neurogenesis by mediating sonic hedgehog signaling. Proc Natl Acad Sci U S A. 2008; 105:13127–13132. [PubMed: 18728187]
44. Davis RE, et al. A knockin mouse model of the Bardet-Biedl syndrome 1 M390R mutation has cilia defects, ventriculomegaly, retinopathy, and obesity. Proc Natl Acad Sci U S A. 2007; 104:19422–19427. [PubMed: 18032602]

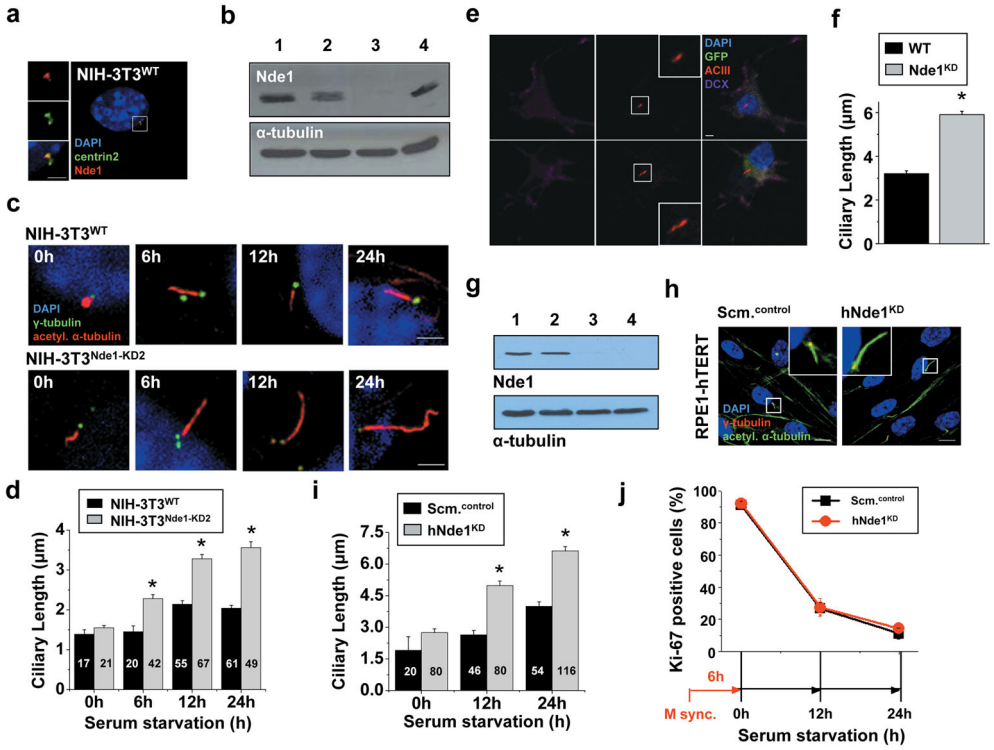

Figure 1.

Depletion of Nde1 induces longer cilia. (**a**) Immunofluorescence staining of centrin2 (green) or Nde1 (red) in NIH-3T3^{WT} cells. (**b**) Expression of endogenous Nde1 in asynchronous cultures of NIH-3T3^{WT} cells (lane 1), NIH-3T3$^{Nde1\text{-}KD1}$ (lane 2), NIH-3T3$^{Nde1\text{-}KD2}$ (lane 3), or NIH-3T3$^{KD\text{-}con.}$ cells (lane 4) (upper panel) or α-tubulin (loading control, lower panel). (**c**) Time course of cilia formation induced by serum starvation in NIH-3T3^{WT} and NIH-3T3$^{Nde1\text{-}KD2}$ cells. Cilia or basal bodies were visualized by an antibody against acetylated α-tubulin (red) or γ-tubulin (green). Scale bar, 2.5 μm. (**d**) Average ciliary length of NIH-3T3^{WT} cells at 0 (n=17), 6 (n=20), 12 (n=55), or 24h of serum starvation (n=61) and NIH-3T3$^{Nde1\text{-}KD2}$ at 0 (n=21), 6 (n=42), 12 (n=67), and 24h (n=49) of serum starvation. Ciliary length was measured from ciliated cells in each group per time-point from a representative experiment. "*", P<0.05, Student's t test. (**e**) DAPI-, doublecortin (DCX)-, and adenylyl cyclase 3 (ACIII)-labeled freshly dissociated, mouse E18.5 embryonic cortical neurons transiently transfected with GFP or GFP plus an Nde1-specific shRNA. Scale bar: 5 μm. (**f**) Average ciliary length of GFP^{+}/DCX^{+} embryonic neurons transiently transfected with GFP alone (n=84) or GFP plus Nde1-specific shRNA (n=76). "*", P <0.05, Student's t test. (**g**) Expression of Nde1 (upper panel) or α-tubulin (lower panel) in untransfected RPE1-hTERT cells (lane 1), RPE1-hTERT cells transiently transfected with a control siRNA for 48h (lane 2), human Nde1-specific siRNA (hNde1 siRNA) for 24h (lane 3), or hNde1 siRNA for 48h (lane 4). (**h**) RPE1-hTERT cells transiently transfected with siRNA control (Scm.^{control}) or siRNA targeting human Nde1 (hNde1^{KD}) were double-stained with antibodies against γ-tubulin (red) and acetylated α-tubulin (green) following 24h serum starvation. Scale bar, 10 μm. (**i**) Average ciliary length of Scm.^{control} at 0 (n=20), 12 (n=46), or 24h (n=54) of serum starvation and hNde1^{KD} RPE1-hTERT cells at 0 (n=80), 12 (n=80),

and 24h (n=116) of serum starvation. Quantification was obtained from ciliated cells. "*",P <0.05, Student's t test. (**j**) Percentage of Ki-67 positive Scm.^{control} or hNde1^{KD} RPE1-hTERT cells synchronized in mitosis by nocodazole treatment (M sync.), followed by a 6h recovery in complete media (0h of serum starvation), followed by serum starvation for 12h or 24h (n=3 independent experiments).

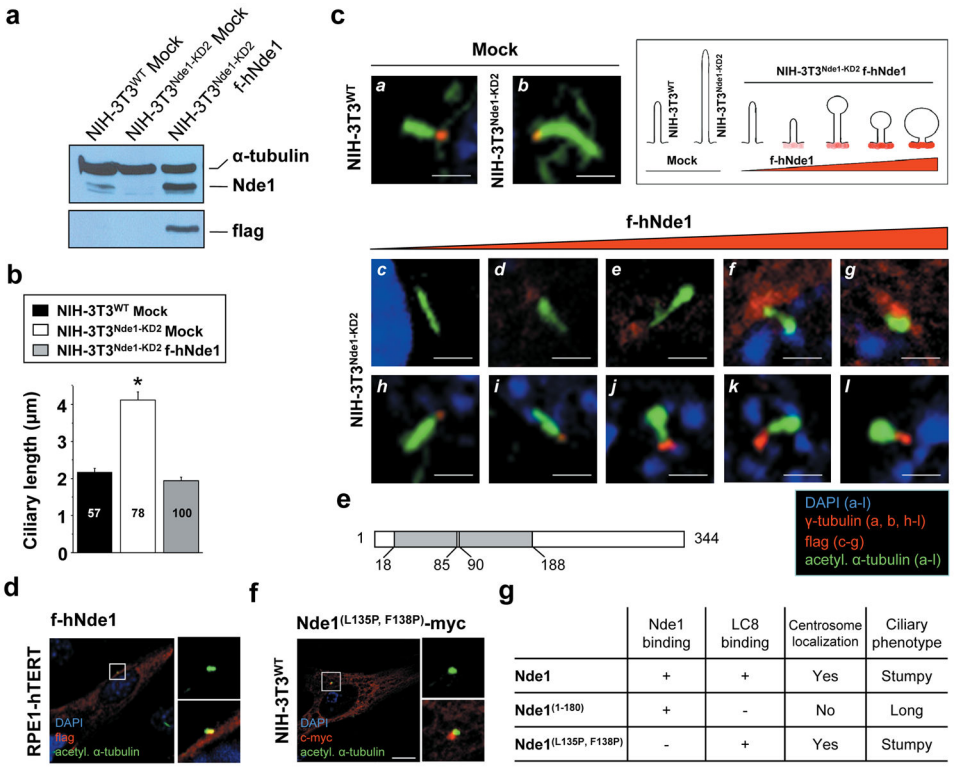

	Nde1 binding	LC8 binding	Centrosome localization	Ciliary phenotype
Nde1	+	+	Yes	Stumpy
Nde1(1-180)	+	-	No	Long
Nde1(L135P, F138P)	-	+	Yes	Stumpy

Figure 2.

Expression of flag-tagged human Nde1 (f-hNde1) rescues abnormally long cilia in NIH-3T3$^{Nde1\text{-}KD2}$ cells. (**a**) Expression levels of f-hNde1 in NIH-3T3$^{Nde1\text{-}KD2}$ cells. Lysates of NIH-3T3^{WT} cells stably expressing GFP (NIH-3T3^{WT} Mock), NIH-3T3$^{Nde1\text{-}KD2}$ cells stably expressing GFP (NIH-3T3$^{Nde1\text{-}KD2}$ Mock) or NIH-3T3$^{Nde1\text{-}KD2}$ cells stably expressing f-hNde1 (NIH-3T3$^{Nde1\text{-}KD2}$ hNde1) were immunoblotted for Nde1 and α-tubulin as loading control (upper panel) or α-flag (lower panel). (**b**) Average ciliary length of NIH-3T3^{WT} cells stably expressing GFP (NIH-3T3^{WT} Mock; n=57), NIH-3T3$^{Nde1\text{-}KD2}$ stably expressing GFP (NIH-3T3$^{Nde1\text{-}KD2}$ Mock; n=78), or NIH-3T3$^{Nde1\text{-}KD2}$ stably expressing f-hNde1 (NIH-3T3$^{Nde1\text{-}KD2}$ hNde1; n=100) following serum starvation for 24h. (**c**) Cilia staining in mock-infected NIH-3T3^{WT} (*a*) and NIH-3T3$^{Nde1\text{-}KD2}$ cells (*b*), or f-hNde1-infected NIH-3T3$^{Nde1\text{-}KD2}$ cells (*c-l*). Antibody against acetylated α-tubulin was used to visualize cilia (*a-l*), antibody against flag to detect f-hNde1 (*c-g*), and antibody to γ-tubulin to visualize the basal body (*a*, *b*, and *h-l*). Note that ciliary morphology and length changed according to the amount of f-hNde1 expressed (*c-g*). (Inset) Schematic representation of the dosage-dependent effect of f-hNde1 on ciliary length and morphology. Low levels of f-hNde1 converted abnormally long cilia back to cilia of normal size (compare *a* with *c*), while moderate or high levels of f-hNde1 resulted in bulged (*d-f*) or stumpy cilia (*g*), respectively. Scale bar, 2.5 μm. (**d**) RPE1-hTERT cells were transiently transfected with f-hNde1 and recovered for 48h followed by an additional 24h of serum starvation. Cells were double-stained with antibodies raised against the flag epitope (red) or acetylated α-tubulin (green). (**e**) Schematic representation of full length Nde1. Coiled-coil domains are shown as grey boxes (18–85 and 90–188). (**f**) Myc-tagged Nde1$^{(L135P,F138P)}$ (Nde1$^{(L135P,\ F138P)}$-myc) was transiently transfected into NIH-3T3^{WT} cells. Cells were

serum starved for 24h and double-stained with antibodies raised against acetylated α-tubulin (green) or the myc epitope (red). Scale bar, 7 μm. (**g**) Summary of structure-function analysis.

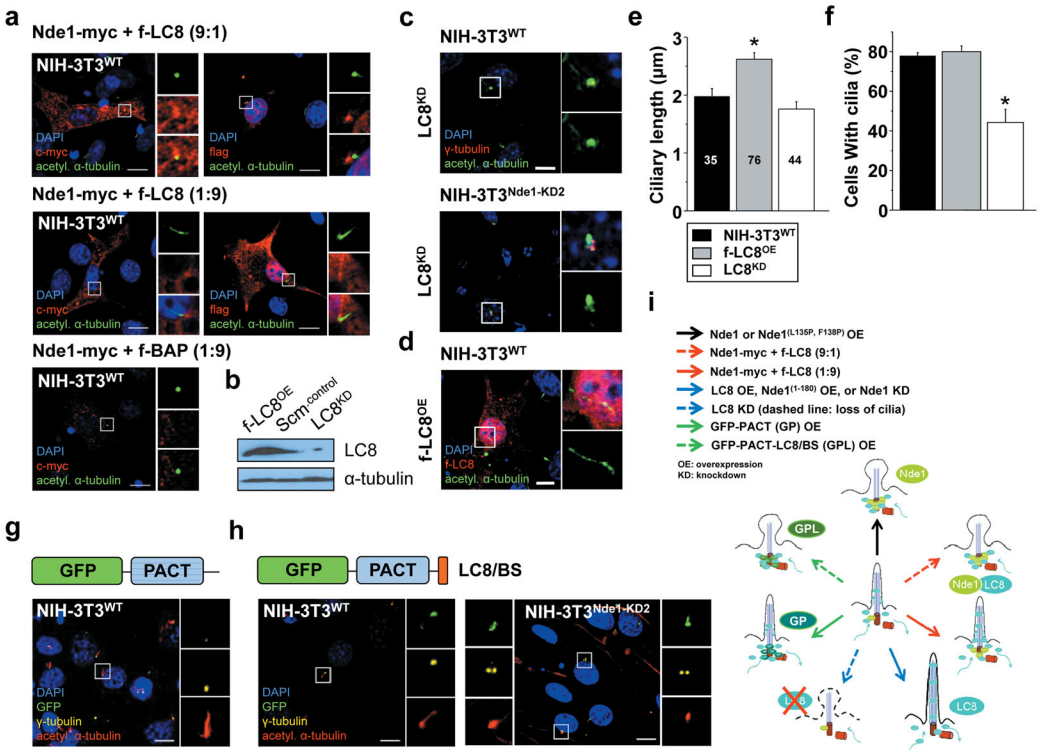

Figure 3.

Nde1 suppresses ciliogenesis through LC8. (**a**) Overexpression of LC8 suppresses the effect of transfected Nde1 on ciliogenesis. NIH-3T3^{WT} cells were transiently co-transfected with wild type Nde1-myc and flag tagged LC8 (f-LC8) at plasmid ratios of 9:1 and 1:9. Co-transfection of Nde1-myc and flag tagged bacterial alkaline phosphatase (f-BAP) in a plasmid ratio of 1:9 was used as control. Scale bar, 7 μm. (**b**) Expression levels of LC8 (upper panel) or α-tubulin (loading control, lower panel) in NIH-3T3^{WT} cells transiently transfected with f-LC8 (f-LC8^{OE}, lane 1), a control siRNA (Scm.^{control}, lane 2), or a mouse LC8-specific siRNA (LC8^{KD}, lane 3). (**c**) Depletion of LC8 suppresses ciliogenesis. NIH-3T3^{WT} and NIH-3T3$^{Nde1\text{-}KD2}$ cells were transiently transfected with LC8-specific siRNA (LC8^{KD}) and double-stained with antibodies against γ-tubulin (red) and acetylated α-tubulin (green), following 24h of serum starvation. Scale bar, 10 μm. (**d**) Overexpression of LC8 promotes cilium formation. NIH-3T3^{WT} cells were transiently transfected with f-LC8 (f-LC8^{OE}) and double stained with an antibody raised against the flag epitope (f-LC8, red) or acetylated α-tubulin (green). Scale bar, 10 μm. (**e** and **f**) Quantification of ciliary length (e) or ciliation (f) of untransfected NIH-3T3^{WT} cells (n=35), transiently transfected with f-LC8 (f-LC8^{OE}, n=76), or LC8-specific siRNA (hNde1^{KD}, n=44). Ciliary length was measured from ciliated cells and percentage of ciliated cells was obtained from three independent experiments (n=3). "*", P <0.05, Student's t test. (**g** and **h**) Artificial tethering of LC8 at the basal body suppresses cilia formation. GFP-PACT (green, g) or GFP-PACT-LC8/BS (green, h) was transiently expressed in NIH-3T3^{WT} and NIH-3T3$^{Nde1\text{-}KD2}$ cells, followed by immunofluorescence staining with γ-tubulin (yellow) or acetylated α-tubulin (red). While both constructs were targeted specifically to the basal body, only GFP-PACT-LC8/BS caused the formation of bulged or stumpy cilia. Scale bar, 10 μm. (**i**) Schematic

diagram summarizing the functional role of Nde1-LC8 interaction in ciliogenesis. Sequestration of LC8 at the basal body suppresses cilia formation, whereas increase of unbound LC8 at the basal body promotes cilia formation.

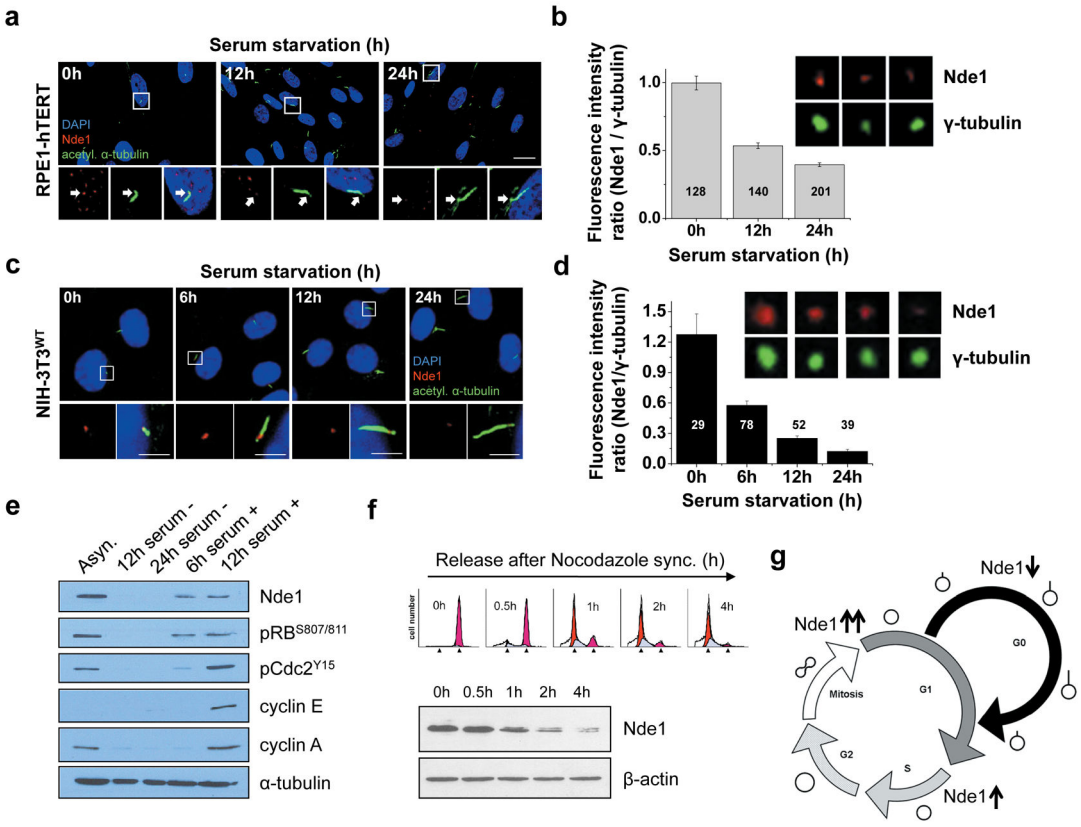

Figure 4.

Nde1 expression inversely correlates with ciliogenesis. (**a** and **c**) Centriolar expression of Nde1 decreases upon ciliation. RPE1-hTERT (a) or NIH-3T3^{WT} (c) cells were serum-starved for the indicated time points. Nde1 (red) or acetylated α-tubulin (green) was visualized by indirect immunofluorescence. Arrows indicate Nde1 localization. Scale bar, 10 μm (a). Scale bar, 2.5 μm (c). (**b** and **d**) Quantification of fluorescence intensity ratio of Nde1/γ-tubulin (red/green) signals at the centrosome at 0 (n=128), 12 (n=140) or 24h (n=201) of serum starvation. Fluorescence intensity of coinciding green or red pixels within the boxed area (inset) was measured in a projection of z series collected in 0.5 μm intervals. The range of fluorescence intensity per pixel in box was from 0–255 (n is indicated on graph). (**e**) Cell cycle dependent regulation of Nde1 expression. Asynchronously proliferating NIH-3T3^{WT} cells (lane 1, Asyn.) were serum starved for 12h (lane 2, 12h serum −), and 24h (lane 3, 24h serum −), followed by serum re-stimulation for 6h (lane 4, 6h serum +), and 12h (lane 5, 12h serum +). Phosphorylation levels of RB (pRB$^{S807/811}$) and Cdc2 (pCdc2^{Y15}) or levels of cyclin A, cyclin E, and Nde1 were determined by immunoblotting. α-tubulin was used as a loading control. (**f**) Nde1 levels decrease as cells exit mitosis. Cell cycle analysis of NIH-3T3^{WT} cells synchronized in mitosis by nocodazole treatment (600ng/ml) for 12h (0h), followed by wash and release into complete media (10% calf serum) for 0.5, 1, 2, or 4h (inset). Lysates from cells arrested in mitosis (0h, lane 1), cells released from mitosis for 0.5 (lane 2), 1 (lane 3), 2 (lane 4), or 4 h (lane 5) were immunoblotted with antibodies against Nde1 (upper panel) or β-actin (lower panel). (**g**) Schematic diagram of Nde1 expression during the cell cycle and ciliogenesis.

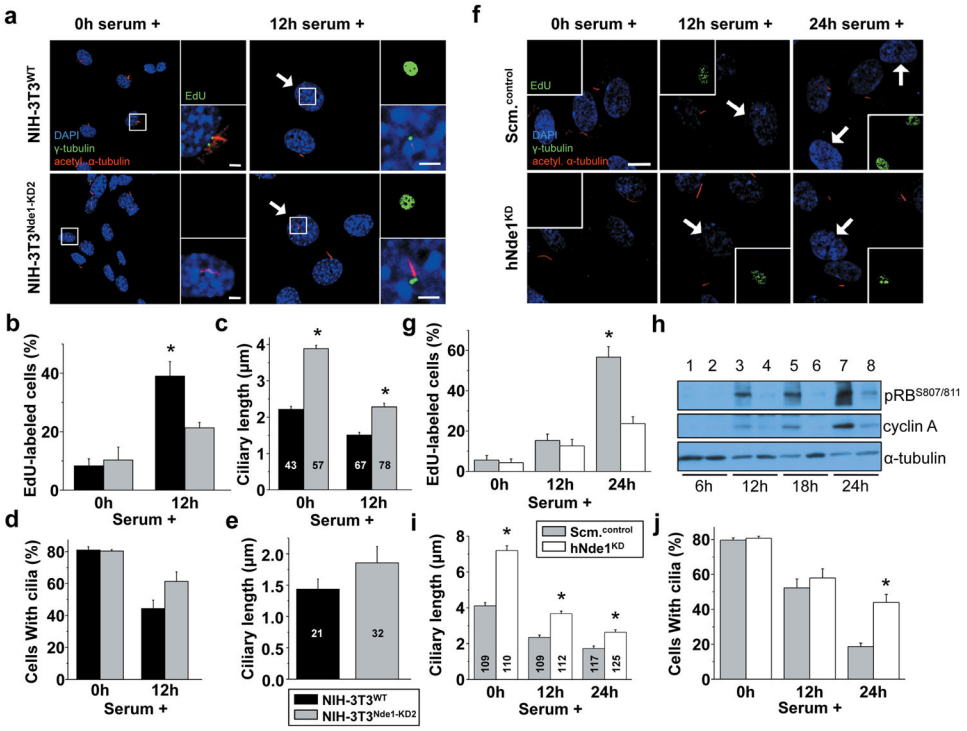

Figure 5.

Nde1 depletion causes a delay in cell cycle re-entry. (**a**) NIH-3T3^{WT} and NIH-3T3$^{Nde1\text{-}KD2}$ cells were arrested in G0 by 24h serum starvation (0h serum +) and induced to re-enter the cell cycle by serum re-stimulation for 12h (12h serum +). Cells were pulse-labeled with EdU and immunostained with antibodies against γ-tubulin (green), acetylated α-tubulin (red), and EdU (green, inset). For illustration purposes, EdU labeling is shown as a 25% reduction of the projected image. Arrows indicate EdU-labeled cells. Scale bar, 2.5 μm. (**b**) Percentage of EdU-positive NIH-3T3^{WT} (black) or NIH-3T3$^{Nde1\text{-}KD2}$ (gray) cells following serum re-stimulation (n=3 independent experiments). "*", P <0.05. Student's t test. (**c**) Ciliary length of NIH-3T3^{WT} (black) at 0 (n=43) or 12h (n=67) of serum re-stimulation and NIH-3T3$^{Nde1\text{-}KD2}$ (gray) at 0 (n=57) or 12 h (n=78) of serum re-stimulation. "*", P <0.05. Student's t test. (**d**) Percentage of ciliated NIH-3T3^{WT} (black bar) or NIH-3T3$^{Nde1\text{-}KD2}$ (gray bar) cells following serum re-stimulation (n=3 independent experiments). "*", P <0.05. Student's t test. (**e**) Ciliary length of EdU-positive NIH-3T3^{WT} (black, n=21) or NIH-3T3$^{Nde1\text{-}KD2}$ (gray, n=32) cells following serum re-stimulation. "*", P <0.05. Student's t test. (**f**) Scm.^{control} or hNde1^{KD} RPE1-hTERT cells were immunostained with antibodies against γ-tubulin (green), acetylated α-tubulin (red), and EdU (green, inset). Arrows indicate EdU-labeled cells. Scale bar, 10 μm. (**g**) Percentage of Scm.^{control} (gray) or hNde1^{KD} (white) RPE1-hTERT cells labeled with EdU at 24h following serum starvation (0h serum +), 12h (12h serum +), and 24h following serum re-stimulation (24h serum +) (n=3 independent experiments). "*", P <0.05. Student's t test. (**h**) Phospho-RB (pRB$^{S807/811}$) and cyclin A levels in Scm.^{control} (lanes 1, 3, 5, and 7) and hNde1^{KD} RPE1-hTERT cells (lanes, 2, 4, 6, and 8) at 6h, 12h, 18h, and 24h following serum re-stimulation (serum +). α-tubulin was used as loading control. (**i**) Ciliary length of RPE1-hTERT Scm.^{control} (gray) at 0 (n=109), 12 (n=109), or 24h (n=117) of serum re-stimulation and hNde1^{KD} (white) at 0

(n=110), 12 (112), or 24h (n=125) of serum re-stimulation. "*", P <0.05. Student's t test. (**j**) Percentage of ciliated Scm.^{control} or hNde1^{KD} RPE1-hTERT cells following serum re-stimulation (n=3 independent experiments). "*", P<0.05. Student's t test.

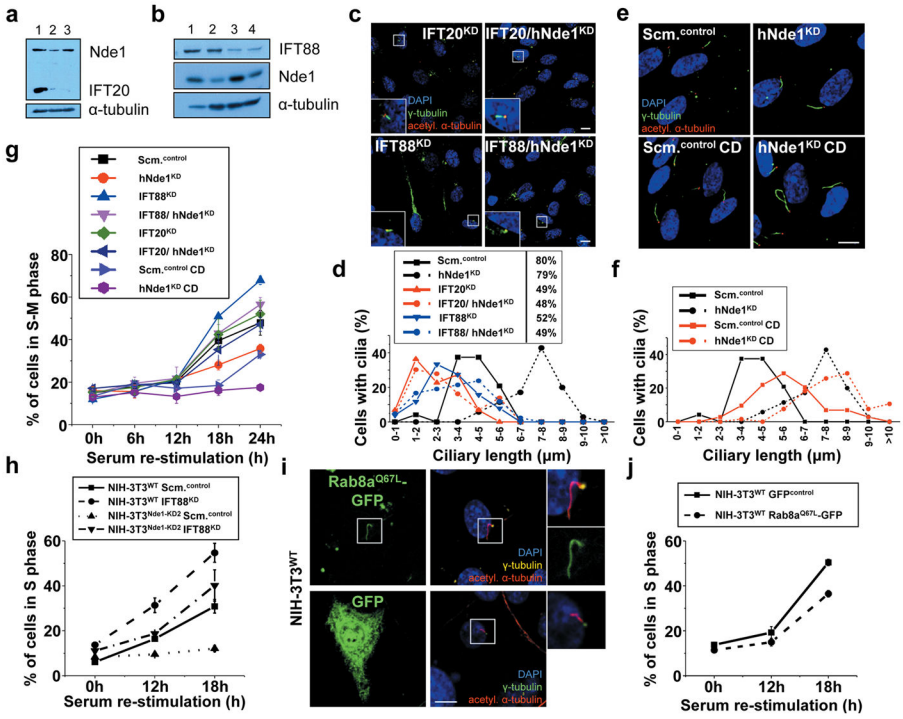

Figure 6.

Knockdown of Nde1 causes a cilium-dependent delay in cell cycle re-entry. (**a**) Expression levels of Nde1 and IFT20 (upper panel) or α-tubulin (loading control, lower panel) in untransfected RPE1-hTERT cells (lane 1), RPE1-hTERT cells stably expressing an shRNAi construct targeting IFT20 (IFT20^{KD}) transiently transfected with an siRNA against hNde1 (lane 2), or IFT20^{KD} cells (lane 3). (**b**) Expression levels of IFT88/polaris (upper panel), Nde1 (middle panel), or α-tubulin (loading control, lower panel) in untransfected RPE1-hTERT cells (lane 1), transiently transfected with a siRNA against hNde1 (lane 2), siRNA against iFT88/polaris (lane 3), or both siRNAs for hNde1 and IFT88/polaris (lane 4). (**c**) RPE1-hTERT IFT20^{KD} (IFT20^{KD}), IFT20/hNde1^{KD}, IFT88^{KD}, or IFT88/hNde1^{KD} cells were double stained with antibodies against γ-tubulin (green) or acetylated α-tubulin (red). (**d**) Cilia length distribution of RPE1-hTERT Scm.^{control}, hNde1^{KD}, IFT20^{KD}, IFT20/ hNde1^{KD}, IFT88^{KD}, and IFT88/hNde1^{KD} cells. Overall percentile of ciliation is shown next to legend. (**e**) RPE1-hTERT cells transfected with a control siRNA (Scm.^{control}) or hNde1 siRNA (hNde1^{KD}) were treated with Cytochalasin D (Scm.^{control} CD or hNde1^{KD} CD) and immunostained with antibodies against γ-tubulin (green) or acetylated α-tubulin (red). (**f**) Cilia length distribution of Scm.^{control}, hNde1^{KD}, Scm.^{control} CD, or hNde1^{KD} CD cells. (**g**) Time course of cell cycle re-entry of Scm.^{control}, hNde1^{KD}, IFT88^{KD}, IFT88/hNde1^{KD}, IFT20^{KD}, IFT20^{KD}/hNde1^{KD}, Scm.^{control} CD, and hNde1^{KD} CD RPE1-hTERT cells in response to serum re-stimulation. (n=3 independent experiments). (**h**) Time course of cell cycle re-entry of NIH-3T3^{WT} cells transfected with a control siRNA (NIH-3T3^{WT} Scm.^{control}) or IFT88/polaris-specific siRNA (NIH-3T3^{WT} IFT88^{KD}) and NIH-3T3$^{Nde1\text{-}KD2}$ cells transiently transfected with control scrambled siRNA (NIH-3T3$^{Nde1\text{-}KD2}$ Scm.^{control}) or IFT88/polaris-specific siRNA (NIH-3T3$^{Nde1\text{-}KD2}$ IFT88^{KD}). (n=3 independent experiments). (**i**) Rab8a^{Q67L}-GFP induces long cilia in NIH-3T3^{WT} cells. GFP- or

Rab8a^{Q67L}-GFP – transfected NIH-3T3^{WT} cells were stained for γ-tubulin (yellow or green) or acetylated α-tubulin (red). Scale bars, 10 μm. (**j**) Time course of cell cycle re-entry of NIH-3T3^{WT} GFP^{control} or NIH-3T3^{WT} Rab8a^{Q67L}-GFP) cells in response to serum re-stimulation. (n=3 independent experiments).

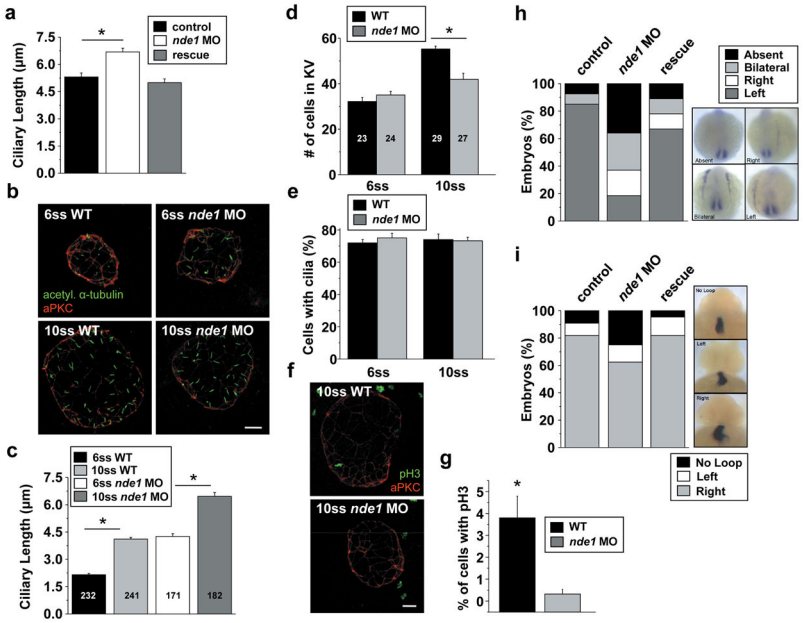

Figure 7.

Depletion of *nde1* in zebrafish leads to longer cilia and smaller Kupffer's vesicle. (**a**) Average ciliary length at 10 somite stages (ss) of wild-type zebrafish embryos (control; n=75), embryos injected with *nde1* morpholino (*nde1* MO; n=100), or co-injected with *nde1* morpholino and human *NDE1* cap mRNA (rescue; n=87). "*",*P* <0.001. Student's *t* test. (**b**) Whole-mount immunofluorescence staining of cilia at the Kupffer's vesicle at 6 or 10ss embryos using acetylated α-tubulin (green) and atypical PKC (aPKC, red) in wild type (WT) embryos (left panels) or *nde1* MO (right panels). Scale bars, 10 μm. (**c**) Average ciliary length in Kupffer's vesicle of WT at 6 (n=232) or 10ss (n=241) embryos and *nde1* MO at 6 (n=171) or 10ss (n=182) embryos. n represents ciliated cells from 6–10 embryos per group. "*", *P* <0.05. Student's *t* test. (**d**) Number of cells in the Kupffer's vesicle in WT (black bar) at 6 (n=23) or 10ss (n=29) and *nde1* MO (gray bar) at 6 (n=24) or 10ss (n=27) embryos. "*", *P* <0.05. Student's *t* test. (**e**) Percentage of ciliated cells in the Kupffer's vesicle of WT (black bar) or *nde1* MO (gray bar) at 6 and 10ss. (n=3 independent experiments). (**f**) Whole-mount immunofluorescence staining of the Kupffer's vesicle of 10ss WT and *nde1* MO with antibodies against phosphorylated histone H3 (pH3, green) or atypical PKC (aPKC, red). Scale bars, 10 μm. (**g**) Percentage of pH3-positive cells in the Kupffer's vesicle of 10ss WT (black bar) and *nde1* MO (gray bar). (n=3 independent experiments). "*", *P* <0.001. Student's *t* test. (**h**) Percentage of embryos in wild-type (control), *nde1* MO, or human *NDE1* mRNA plus *nde1* MO co-injected embryos (rescue) with no expression of *southpaw* (Absent), expression at the right side (Right), left side (Left), or expression on both sides (Bilateral) of the lateral plate mesoderm at 14 hpf. Dorsal view of *southpaw* mRNA at 14 hpf. (**i**) Percentage of embryos in each group with no looping (No loop), leftward (Left), or rightward looping (Right) of the heart tube at 48 hpf determined by the expression pattern of *myl-7* mRNA. Laterality defects are manifested as non-looping (No Loop) or leftward looping (Left), whereas wild-type embryos show rightward looping of the heart (Right).